

Using Surface Plasmon Resonance Imaging to Probe Dynamic Interactions Between Cells and Extracellular Matrix

Alexander W. Peterson,* Michael Halter, Alessandro Tona, Kiran Bhadriraju, Anne L. Plant

Cell System Science Group, Biochemical Sciences Division, National Institute of Standards and Technology, Gaithersburg, MD

Additional Supporting Information may be found in the online version of this article.

Received 8 October 2009; Revision Received 3 June 2010; Accepted 7 June 2010

*Correspondence to: Alexander W. Peterson, Cell Systems Science Group, Biochemical Science Division, National Institute of Standards and Technology, 100 Bureau Drive, Stop 8313, Gaithersburg, MD 20899-8313

Email: alexander.peterson@nist.gov

Published online 13 July 2010 in Wiley Online Library (wileyonlinelibrary.com)

DOI: 10.1002/cyto.a.20938

Published 2010 Wiley-Liss, Inc. †This article is a US government work and, as such, is in the public domain in the United States of America.

• Abstract

Spatially resolved details of the interactions of cells with a fibronectin modified surface were examined using surface plasmon resonance imaging (SPRI). SPRI is a label-free technique that is based on the spatial measurement of interfacial refractive index. SPRI is sensitive to short range interactions between cells and their substratum. The high contrast in SPR signal between cell edges and substratum facilitates identification of cell edges and segmentation of cell areas. With this novel technique, we demonstrate visualization of cell-substratum interactions, and how cell-substratum interactions change over time as cells spread, migrate, and undergo membrane ruffling. Published 2010 Wiley-Liss, Inc.†

• Key terms

vascular smooth muscle cells; fibronectin; imaging; image analysis; label-free; surface plasmon resonance; cell spreading; ruffling

THE extracellular matrix (ECM) is primarily composed of insoluble proteins surrounding cells, which serves to provide mechanical support and anchorage for cells as well as specific chemical and mechanical cues. The ECM influences intracellular signaling pathways and cytoskeletal organization, and is involved in regulating a cell's dynamic behavior (1–3). A critical challenge in cell biology is tracking and quantifying the interactions of cells with the ECM.

Direct visualization and measurement of cell-ECM interactions are possible using a limited number of optical techniques such as total internal reflection fluorescence microscopy (TIRFM). TIRFM is a fluorescent-based measurement that employs an evanescent wave of excitation light to selectively excite regions of cell-substratum contact. It requires fluorescent labeling of the cell-membrane (4), the cell cytosol (5), or the ECM proteins. Interference reflection microscopy allows label-free measurement of cell-substratum interaction, but the required optical architecture limits the field of view to small, single-cell regions, and the complex optical response precludes quantitation of mass or molecular density (6). Optical waveguides have been used as a label-free measurement technique to quantify cell spreading (7) and is sensitive to cell-secreted materials (8), but it does not provide visualization of cellular features.

Here we demonstrate the use of surface plasmon resonance imaging (SPRI) to spatially resolve and quantitatively analyze both the ECM proteins and the dynamic behavior of live cells. Surface plasmon resonance (SPR) is a label-free evanescent wave technique that is essentially a highly sensitive refractive index measurement near a metallic surface (9). In a nonimaging mode, SPR spectroscopy has been demonstrated as a highly useful and sensitive technique for quantitative determinations of time-dependent changes of binding of proteins (10) and DNA (11) to surface immobilized capture agents. It has been reported that even changes in the dielectric

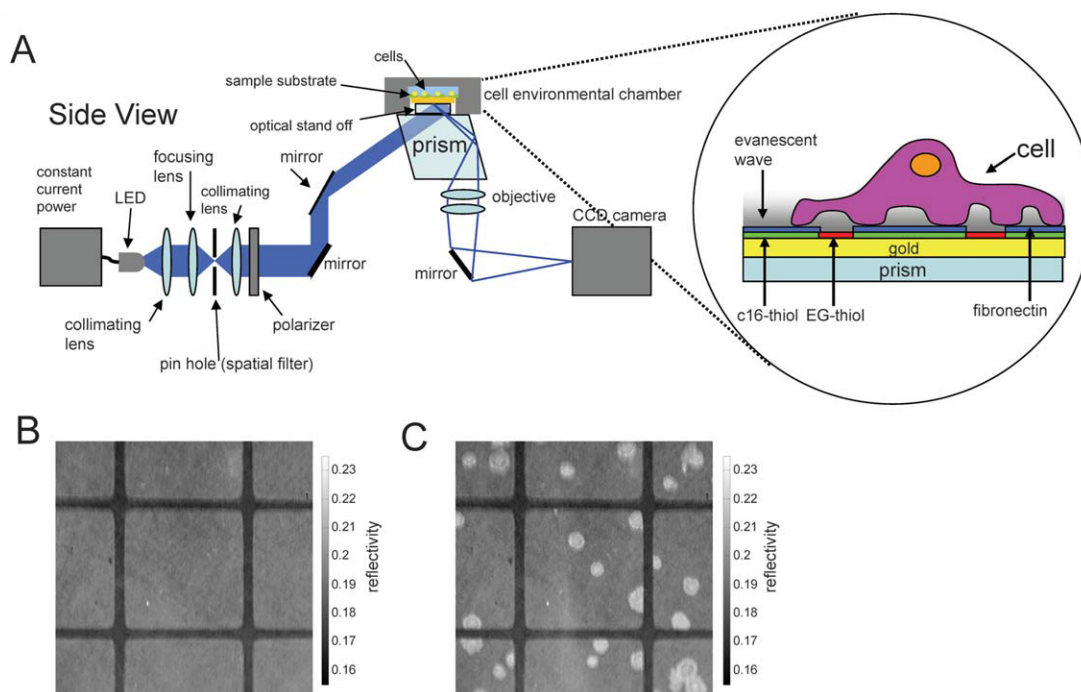


Figure 1. SPRI apparatus layout, interface schematic and representative fibronectin patterned surface before and after cell attachment. **(A)** SPRI imaging instrument layout. About 470-nm light is collimated, spatially filtered, polarized, and directed by mirrors to be incident upon an SF-10 prism and glass slide enclosed in a cell environmental chamber. Reflected light is imaged and recorded on a CCD camera. Inset shows a cartoon of the interface that is measured by the plasmon generated evanescent field: gold coated glass slide, hexadecanethiol/EG microcontact printed surface, fibronectin adsorption onto hexadecanethiol, and subsequent cell adhesion. **(B)** Representative SPRI images. The first image is a SPR reflectivity image of a fibronectin patterned surface where a monolayer of fibronectin was adsorbed onto a $500 \mu\text{m}^2$ features patterned with hexadecanethiol and separated by $50\text{-}\mu\text{m}$ lines backfilled with EG-thiol. The second image is the same field of view 2 h after cell seeding and attachment. [Color figure can be viewed in the online issue, which is available at wileyonlinelibrary.com.]

composition of the cell membrane in cells at a surface can change the SPR response measured using infrared SPR (12). Using SPR in an imaging mode for arrayed analysis of proteins and DNA has been demonstrated (13) as well as using SPR to enhance fluorescence measurements in a TIRF configuration (14,15). There have been only initial attempts reported in the literature by others to image cells with SPRI (16,17). In a previous report from this lab, we demonstrated the use of SPRI to analyze fixed cells and quantify extracellular proteins (18).

In this study, we generate SPRI images of cells with the use of a simple set-up consisting of a prism, visible light, an objective lens and a CCD camera. Using differences in refractive index to provide image contrast, we demonstrate the use of SPRI to image live cells and examine the dynamics of the interactions between cells and their substratum without the need for fluorescent labels. We use SPRI to measure rates of membrane ruffling, cell spreading, and cell-substratum interaction as a function of surface chemistry.

MATERIALS AND METHODS¹

Surface Plasmon Resonance Imaging Apparatus

The SPRI apparatus is diagramed in Figure 1A. The SPRI apparatus has been described previously (18). Briefly, a cell cul-

¹Certain commercial products are identified to adequately specify the experimental procedure; this does not imply endorsement or recommendation by NIST.

ture chamber (FCS2; Biopetech, Butler, PA)¹, was mounted on top of a SF-10 rhomboid prism (Optical Fabrication Shop, NIST, Gaithersburg, MD). An “optical stand-off” (SF-10 glass slide) was designed to couple between the bottom of the FCS2 Biopetech chamber window, a modified gold coated SF-10 glass slide, with the top of the SPR prism. SF-10 index matching fluid, $n = 1.725$ (Cargille Laboratories, Cedar Grove, NJ), was used to optically couple each interface. A power supply (Wavelength Electronics, Bozeman, MT) was used to power a $470 \pm 5\text{-nm}$ LED (LSDiodes, Lake Oswego, Oregon). The incoherent light was collimated, spatially filtered through a pin hole, recollimated, passed through a linear polarizer (Newport, Irvine, CA), and directed to the prism imaging surface at the incident angle of 56° by two broadband dielectric mirrors (Thorlabs, Newton, NJ). The reflected SPR image was collected by two achromatic lenses (Thorlabs, calculated $\text{NA} = 0.38$) and captured by a 12-bit ($2048 \text{ pixel} \times 2048 \text{ pixel}$) Retiga 4000 CCD camera (Qimaging, Surrey, Canada). Images were collected with Qimaging software and 1 pixel equals $\sim 1 \mu\text{m}^2$. The configuration allows the cell chamber to be easily transferred between the SPRI imaging apparatus and an inverted optical microscope.

Substratum Preparation

SF-10 glass slides ($25 \times 25 \times 1 \text{ mm}^3$) (Schott, Elmsford, NY) were acid-washed with 7:3 $\text{H}_2\text{SO}_4:\text{H}_2\text{O}_2$ (19), rinsed with

18 M Ω cm distilled water, rinsed with ethanol, dried under a N₂ stream, and then coated with \sim 1 nm chromium and \sim 30 nm gold by magnetron sputtering using an Edwards Auto 306 vacuum system (Edwards, Wilmington, MA) at 1×10^{-7} mbar. Polydimethylsiloxane (PDMS) stamps with $500\text{-}\mu\text{m}^2$ features spaced $50\ \mu\text{m}$ apart were used for microcontact printing. Masters for casting PDMS, Sylgard 184, (Dow-Corning, Midland, MI) stamps were made using the dry film resist technique and PDMS stamps were cast from these (20). Microcontact printing to the gold substratum was performed according to published procedure (21) using 2-mM hexadecanethiol (Aldrich, St. Louis, MO) in ethanol, resulting in $500\ \mu\text{m}^2$ areas modified with alkanethiol. Following this, the slides were immersed into a 0.5-mM solution of ethylene glycol-terminated alkylthiol, HS(CH₂)₁₁(OCH₂CH₂)₃OH (Aseblon, Seattle, Washington), in ethanol for 12 h to make the remaining areas protein resistant. The hexadecanethiol coated regions have been measured by SPRI to be $\sim 2 \pm 0.08\text{-nm}$ thick (22). Fibronectin was allowed to adsorb onto the alkanethiol patterned areas by placing slides into a sterile solution of 25 $\mu\text{g}/\text{mL}$ bovine plasma fibronectin (Sigma, St. Louis, MO) in Ca²⁺- and Mg²⁺-free Dulbecco's phosphate buffered saline (DPBS; Invitrogen, Carlsbad, CA) for 1 h. The kinetics of fibronectin adsorption to the hexadecanethiol coated regions was determined previously by SPRI (18). The surface density of fibronectin was determined to be $390 \pm 3\ \text{ng}/\text{cm}^2$ which corresponds to $\sim 3 \pm 0.03\text{-nm}$ thickness (18) for a total thickness of material of 5 nm.

The attenuation length (the distance the plasmon field falls to 1/e) for an evanescent wave of plasmons generated by 470-nm light was calculated to be 60 nm (9) (Supplementary Fig. 1). This value, commonly referred to as the penetration depth, is the distance at which the field strength decays to 37% of its original strength. A penetration depth of 60 nm suggests that the SPR signal will be sensitive to several stacked molecular layers as well as the cell membrane and some intracellular material. The inset in Figure 1A shows a cartoon schematic of the prepared patterned substratum. It should also be noted that objects which are more distant than 60 nm can contribute to detectable signal dependent on the detection threshold of the instrument set up. For this experimental setup we estimate that we are sensitive to features residing up to $\sim 180\ \text{nm}$ away from the surface, a distance where the field strength decays to 5% (Supplementary Fig. 1). A similar description for a TIRF system using 480-nm wavelength of evanescent light has been made where the penetration depth is 125 nm (23).

The data in Figure 1B, showing a SPR image of a patterned fibronectin coated surface, provide an indication of the sensitivity of the system. The $500\text{-}\mu\text{m}^2$ regions of fibronectin have a reflectivity value of $\sim 0.19 \pm 0.004$ and the $50\text{-}\mu\text{m}$ lines of EG-thiol have a reflectivity value of $\sim 0.16 \pm 0.004$. The two materials have a similar refractive index and a height difference of only 3 nm, yet these areas are easily distinguishable. The second image, Figure 1C, shows the same patterned surface 2 h after seeding with vascular smooth muscle cells (vSMC). The vSMC have a reflectivity value of $>0.2 \pm 0.004$.

As can be seen, each region of EG, fibronectin and cells has distinct reflectivity values which help to enable image segmentation based on intensity value. SPR images subsequently presented here are cropped images used to focus on specific regions of interest or cells and do not always show the entire patterned surface.

Gelatin/Agarose Beads

A saline suspension of gelatin beads with 4% cross-linked agarose (Sigma, St. Louis, MO) with size distribution (40–165 μm) was diluted 1/20 into DPBS (Invitrogen) and then added to the fibronectin patterned substratum at room temperature.

Cell Culture and Seeding

The rat aortic vSMC line (A10; ATCC, Manassas, VA) was maintained in Dulbecco's Modified Eagles Medium (DMEM; Mediatech, Herndon, VA) supplemented with nonessential amino acids, glutamine, penicillin (100 units/mL), streptomycin (100 $\mu\text{g}/\text{mL}$), 10 % by volume FBS (Invitrogen, Carlsbad, CA) and 25-mM HEPES, and maintained in a humidified 5% CO₂ balanced-air atmosphere at 37°C. Cells were removed from tissue culture polystyrene flasks by trypsinization, and seeded in culture medium onto the fibronectin patterned substratum mounted in a FCS2 environmental chamber (Bioprotech, Butler, PA) at a density of 2,000 cells/cm² and kept at 37°C for the duration of the experiment.

Phase Contrast and Oblique Bright Field Microscopy

Phase contrast microscopy images were acquired using a 10 \times /0.3 NA objective on a Zeiss Axiovert 200 inverted microscope (Carl Zeiss MicroImaging, Thornwood, NY) and a CoolSNAP HQ CCD camera (Roper Scientific, Tucson, AZ). Oblique bright field microscopy (24) images were acquired using a 10 \times /0.25 NA objective on an Olympus IX70 inverted microscope (Center Valley, PA) with a CoolSNAP HQ CCD camera (Roper Scientific). The corresponding SPR images in Figures 1 and 2 were registered to either the phase contrast or oblique image using six fiducial marks.

Surface Plasmon Resonance Imaging Analysis

For SPR imaging, p- and s-polarized light images were taken at 470 nm by rotating the linear polarizer 90°. The p-image was divided by s-image to provide an image that is in units of reflectivity. The p-polarized light is adsorbed by the surface plasmons and provides the image contrast based upon refractive index differences in the surface sample (25). The s-polarized light does not interact with the surface plasmons and remains proportional to incident light intensity; however, it is affected by spatial inhomogeneities in the light source (18). Therefore, dividing the p-polarized image by the s-polarized image provides an effectively normalized image that is in units of reflectivity (0–1) as well as corrects for spatial inhomogeneities due to the illumination source. For live cell time-lapse, paired images were taken with p- and s-polarized light

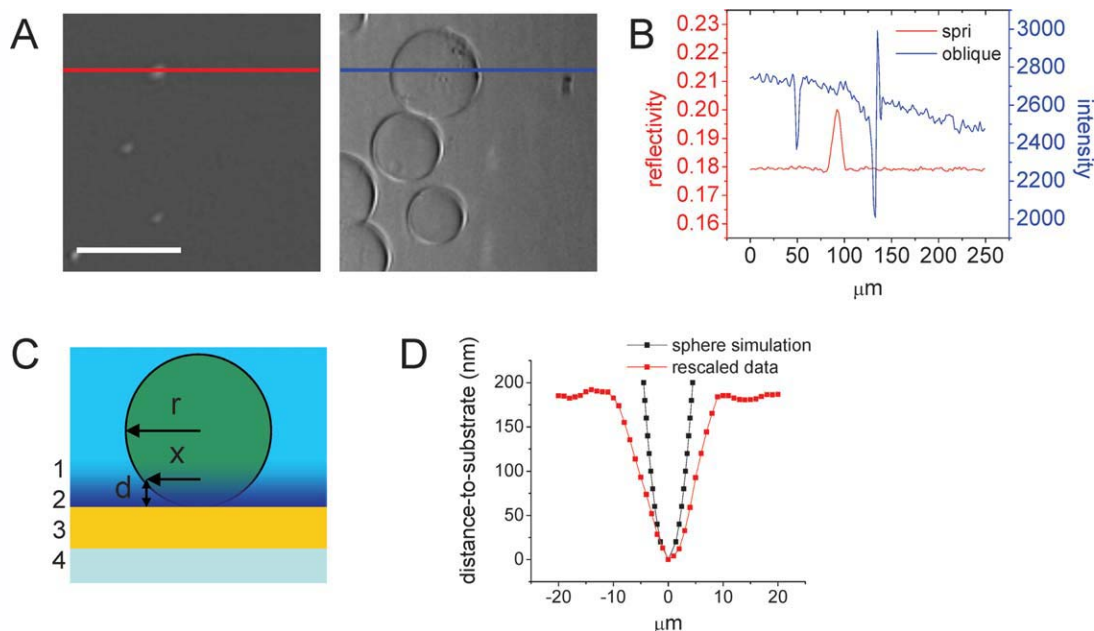


Figure 2. Comparison of gelatin beads using SPRI and oblique imaging and sphere geometric model. **(A)** SPRI of a gelatin/agarose bead (left) compared with oblique bright field imaging (right). Scale bar = 100 μm . **(B)** Reflectivity and brightness values for the pixels under the colored lines in **(A)** that show that SPRI provides a footprint indicating where the bead is in very close proximity to the surface (left) in comparison with the image of the edge of the bead that is provided by oblique imaging (right). **(C)** Schematic illustration of the physical layers that are responsible for the observed SPRI signal of a sphere where (1) is the buffer solution and (2) is the evanescent wave penetration into the solution at the interface of the gold film (3) on the glass prism and (4) r is the radius of the sphere and x is the distance from the center of the sphere to the edge at the farthest point on the sphere that is within the penetration depth, d , of the plasmon evanescent wave. **(D)** The sphere simulation is presented as a distance to substratum and compared with a linear rescaling of the reflectivity data shown in **(B)**. [Color figure can be viewed in the online issue, which is available at wileyonlinelibrary.com.]

at the beginning and end of the experiment while only p-polarized light was used for the time-lapse imaging. Image skew, in Figures 3–5, was corrected by dividing the y -direction of the image (the direction of lateral plasmon propagation and image illumination) by $1/\cos(\theta)$ where $\theta = 56^\circ$ for the angle of incident illumination (18). Live-cell time-lapse images presented in Figures 1, 2, and 5 are displayed as reflectivity intensity values as indicated by the scalebar or corresponding line scan.

Live cell time-lapse images presented in Figures 3 and 4 are displayed as “difference images” overlaid on the time-lapsed reflectivity image. This analysis routine is performed to display pseudocolored cell features on top of grey scale fibronectin/PEG features. The difference images are generated by applying a threshold of ΔR values >0.01 for intensity values attributed to cell features (described in Supplementary Fig. 2), and all lower ΔR values are considered noncell protein and PEG background; the cell features are displayed in pseudocolor and the protein and PEG features are displayed in grayscale. In sequence, the images after seeding are a difference image subtracting the initial ($t = 0$ min) image. This creates an image that depicts change in reflectivity (ΔR). Because ΔR values of cell features are large compared with those for non-cell protein and PEG features, a threshold of $\Delta R > 0.01$ is used to select cell features. The specific SPRI reflectivity threshold value used to segment cells was made in comparison with registered phase contrast images (18). The ΔR values for

the cell features are mapped to a pseudocolored scale. The time-lapse ΔR images are then overlaid onto the corresponding time-lapse reflectivity image resulting in a hybrid image consisting of pseudocolored ΔR values on top of a grayscale reflectivity image.

Binary masks are made from these images to label individual cells and measure spread area. For Figure 4, the binary mask of the cell object is multiplied by masks generated by the threshold of PEG/fibronectin substratum in the first image frame. From this, the spread area of the cell was measured on both the PEG and fibronectin regions (see Supplementary Movie 3). For the lateral ruffling measurements (Fig. 5), the center of the cell lamellipodia was manually tracked over 25 min (five time-lapse frames) and the distance travelled was averaged and reported in units of $\mu\text{m}/\text{min}$.

All image analysis was performed using code written in MATLAB and functions provided in MATLAB Image Processing Toolbox (Mathworks, Natick, MA).

RESULTS

Surface Plasmon Resonance Imaging Reports Distance of Object from the Surface

The gold substratum used in SPRI allows for surface functionalization with self-assembled monolayers formed by alkanethiols, which provides a method for patterning with extracellular matrix proteins and tailoring the substratum for

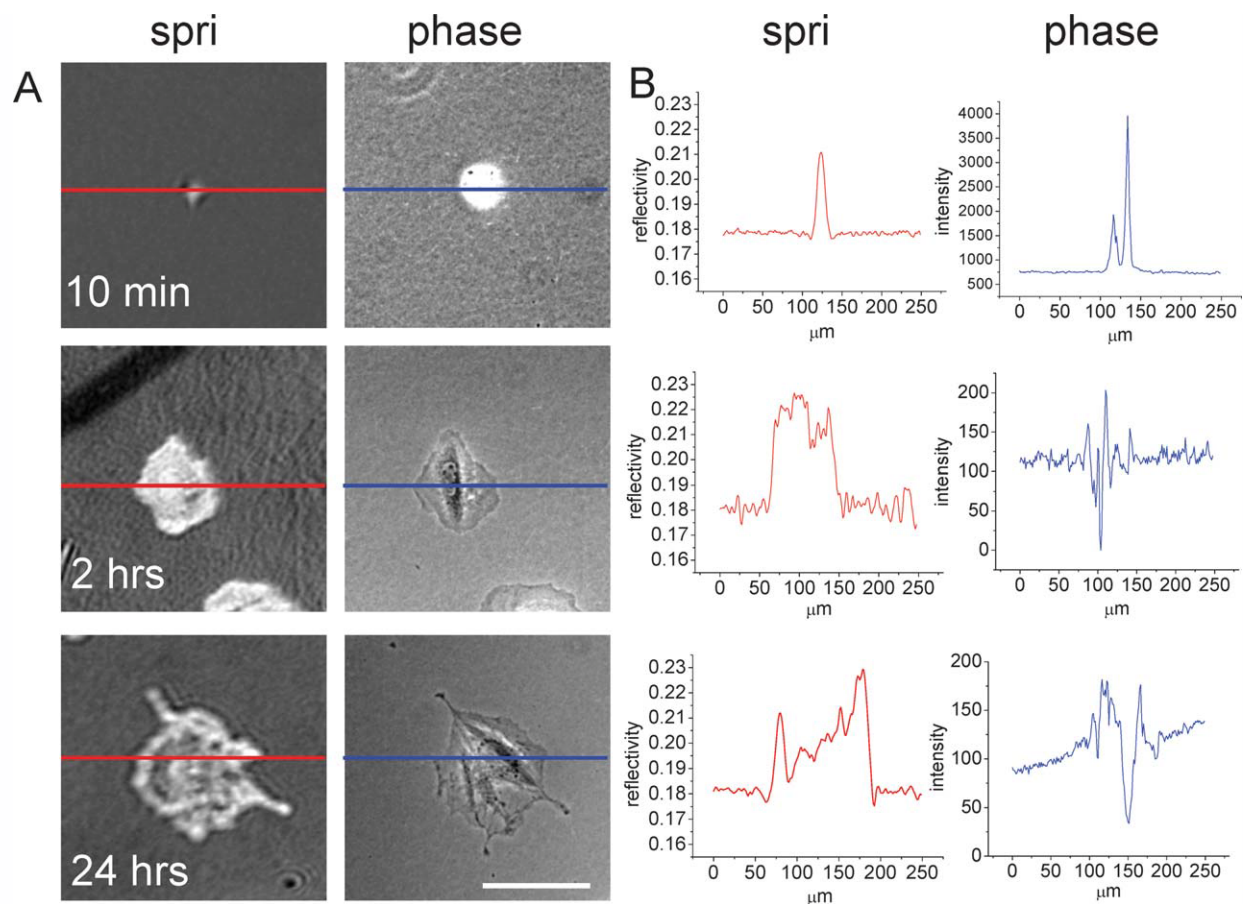


Figure 3. Comparison of vSMC cell spreading using SPRI and phase contrast. **(A)** Ten minutes after the addition of cells to the substratum, SPRI shows a smaller cell footprint than phase contrast images. At 2 h of spreading, the cell perimeter appears similar in the SPRI and phase contrast images. After 24 h, the SPR image indicates that the cell interaction with the substratum is more heterogeneous than it was at 2 h. **(B)** Line scans from **(A)**. A smaller cell profile in SPRI is shown at 10 min. At 2 h, a line scan through the cell shows a large reflectivity signal in SPRI that is relatively homogenous throughout the cell. The profile through the SPRI cell image shows a larger reflectivity signal variation at 24 h than 2 h. Scale bar = 100 μm . [Color figure can be viewed in the online issue, which is available at wileyonlinelibrary.com.]

cell biology (26). The gold layer also serves as the SPR sensor since it serves as the source of the plasmon field. SPR is an electromagnetic phenomenon that is highly sensitive to the metal layer at an interface, the difference in refractive index at

that interface, and the wavelength and incident angle of the light (9). The evanescent wave of excited plasmons resides close to the gold/liquid interface. The attenuation of plasmons at the surface is a function of the refractive index and mass of

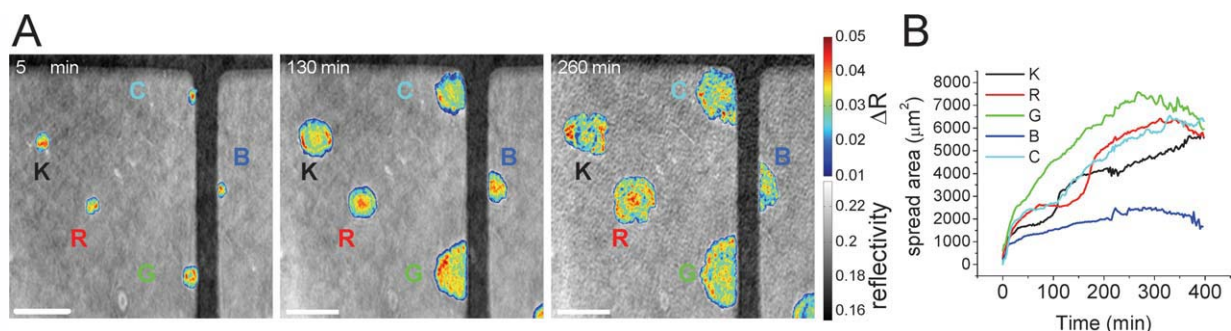


Figure 4. Time dependent measurements of cell spreading using SPRI. **(A)** Selected frames of time-lapse imaging of vSMC spreading onto a 500 μm^2 of fibronectin (grey areas) separated from other fibronectin areas by PEG (dark lines). **(B)** Cell spreading was quantified for individual cells over time. The hybrid color bar represents combined reflectivity and ΔR (reflectivity change) values taken using SPRI difference imaging. Scale bars = 100 μm . [Color figure can be viewed in the online issue, which is available at wileyonlinelibrary.com.]

material at the surface, convoluted by the distance the material is away from the surface.

To aid in the interpretation of SPRI data from a sample such as a cell, that is thick relative to the penetration depth of the plasmon wave, we performed preliminary measurements using gelatin beads as a model system. Figure 2A shows a field of gelatin beads that were allowed to deposit onto the fibronectin coated substratum and were imaged by both SPRI, which is a reflectance and transmission technique, and an oblique illumination (27). In the SPRI image, the beads appear very small because only the portion of each bead that is sufficiently close to the surface to be within the penetration depth of the plasmon wave is being detected, while oblique illumination shows an image of beads of expected diameter ($\sim 75 \mu\text{m}$). Figure 2B shows the corresponding line scans of intensities in the two images. We assume that the beads are effectively homogeneous in composition and the refractive index is constant throughout the bead. As a result, and because of the sensitivity of the intensity of the plasmon evanescent wave to distance from the surface, the reflectivity intensity of the bead in the SPR image is related to the distance that different parts of the bead are from the substratum. Figure 2C illustrates the relationship between the bead radius (r) as observed by oblique illumination, the apparent bead radius observed by SPR (x), and the distance (d) that the apparent edge of the sphere (as visualized by SPR) resides above the substratum. The measured apparent radius, x , of the bead based on the SPR image is $\sim 20 \mu\text{m}$ and the equation relating these variables is:

$$d = r - \sqrt{r^2 - x^2}$$

The data in Figure 2B, which shows the measured reflectivity of the bead as a function of x -axis position in the image in Figure 2A, was used to determine the distance of the bead surface from the substratum. This is plotted as the red line in Figure 2D. The highest reflectivity occurs where the bead is in direct contact with the substratum; due to the curvature of the bead, other points on the bead are farther away from the surface. The data in Figure 2B, which are reported in reflectivity units, are converted in Figure 2D into units of distance to substratum by assuming that the evanescent wave of the plasmon field effectively extends into the medium a maximum of 180 nm, which represents an estimated detection threshold at the point the field decays to less than 5% (Supporting Fig. 1). For comparison, we present simulated data that would be expected from a perfectly spherical bead (Fig. 2D, black line). The difference between these plots indicates that the SPR signature of the bead falls off more gradually than would be anticipated from a perfect sphere, suggesting that the gelatin bead may be deforming at the surface. This is reasonable since fibronectin is known to bind strongly with gelatin (28,29). In fact, once the beads deposit on the surface they do not move when rinsed, indicating that the beads adhere to the fibronectin coated substratum. The gelatin beads with their homogeneous refractive index provide insight into how SPR images are influenced by distance from

the surface, and provide a basis for interpreting the reflectivity signal of large objects, such as adherent mammalian cells, whose mass exists within and extends beyond the penetration depth of the evanescent plasmon wave.

Surface Plasmon Resonance Imaging and Phase Contrast Imaging of Cell Adhesion and Spreading

Figure 3 shows vSMC after their addition to a patterned fibronectin modified surface. At 10 min after seeding cells, the SPR image is quite different from the phase contrast image of the same cell (Fig. 3A). The SPR image shows the footprint of the cell that is in close contact with the substratum, which is significantly smaller than the cross-section of the cell revealed by phase contrast imaging. This is similar to observations made on the gelatin bead described above in that the cell apparently associates with the substratum as a sphere-like body. The corresponding line scan (Fig. 3B) of the SPR reflectivity profile depicts a single maximum reflectivity and an apparent width of $15 \mu\text{m}$, in contrast to the phase contrast image which shows both light and dark cell features due to the different modes of contrast generation by the two methods. The outer edges of the cell object in the phase contrast image appear to be $40 \mu\text{m}$ apart. After 2 h of spreading, the location of the cell edges appears similar in the SPR and phase contrast images. However, while the phase contrast image has both bright and dark features compared with background, a typical characteristic that makes image segmentation with a single threshold challenging, the SPR image has a positive shift in reflectivity intensity due to the refractive index contribution of the cell at the substratum. In addition, the cell image has a higher signal-to-noise with SPR imaging compared with the phase image as can be seen in the line scan profiles (Fig. 3B). These characteristics facilitate the segmentation of cell objects in SPR images.

It is interesting to note that the SPR image indicates a fairly homogeneous cell-substratum footprint at 2 h; however, at 24 h, the overall variation in SPR signal intensity of the cell is larger and the cell footprint is more heterogeneous. An apparent decrease of cell-substratum homogeneity with time was observed frequently in this study, and is consistent with trends observed for fibroblasts measured by scanning electron microscopy and interference reflection microscopy (30). This change in the SPR image indicates either changes in the cell-substratum distance at different points in the cell and/or changes in cellular protein organization proximal to the membrane, over time. Change in protein organization could arise from the maturation of focal adhesions inside the cell and/or the secretion of ECM proteins.

Surface Plasmon Resonance Imaging of Live Cell Spreading and Ruffling

The data presented above indicate that SPRI appears to be highly sensitive to cell adhesions. An advantage of SPRI is the ability to observe and quantify live cell morphology, movement, and interaction with its ECM with minimal perturbation of the cells such as addition of a fluorescent dye. The results of live cell imaging with SPRI are shown in Figure 4. The rate of spreading of individual cells was followed in

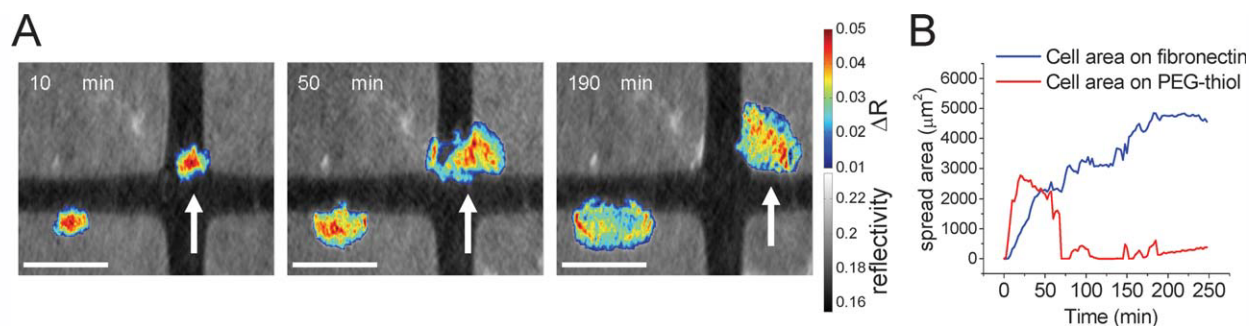


Figure 5. Time dependent measurements of cell spreading and interaction with substratum. **(A)** Time-lapse images of an individual cell (arrow) moving from a PEG-thiol patterned region (dark lines) onto a fibronectin patterned region (grey). **(B)** Spread area for the cell in **(A)** quantified as a function of substratum identity, PEG versus fibronectin. The hybrid color bar represents combined reflectivity and ΔR (reflectivity change) values taken using SPRI difference imaging. Scale bars = $100 \mu\text{m}$. [Color figure can be viewed in the online issue, which is available at wileyonlinelibrary.com.]

real time. Cells were observed for more than 6 h beginning immediately after seeding them onto fibronectin which was patterned in $500 \mu\text{m}$ by $500 \mu\text{m}^2$ (Fig. 4A). Cell attachment and spreading was observed in time-lapse SPRI difference images (Fig. 4A, Supplemental Movie 1). An SPR intensity value was chosen as a threshold intensity, above which pixels were considered to belong to cells. The large intensity differences between cells and background, such as shown by the data in Figure 3B, make this an unambiguous operation, and allow determination of individual cell contours. Figure 4B shows the time course for change in cell spread areas for five selected cells. Cell spread area steadily increases until it stabilizes after ~ 300 min; fully spread cells ranged in area from $2,000$ – $7,000 \mu\text{m}^2$ per individual cell. Because of the high fibronectin surface density, each cell shown in Figure 4A spread in the initial spot it adhered to, with very little migration (31). Cells did not spread onto the EG-thiol coated regions, an observation made possible because the SPR images indicate both the positions of the cells and the underlying protein patterns (Figs. 3A and 4A).

SPRI has a distinct advantage over other imaging modalities in that, while it can report on cells and their interaction with substratum, it can also provide information about the substratum itself, even when that substratum is a monolayer of protein. Figure 5 shows the behavior of a cell on the nonadhesive EG-coated area of the substratum during initial cell seeding. The darker EG-coated area is easily distinguished from the brighter fibronectin coated squares. Figure 5A shows a cell that initially contacted the EG-thiol region and then migrated onto a fibronectin region. The cell initially contacted only the EG-thiol, and after several minutes extended lamellipodia onto the fibronectin. As can be seen in the video file (Supplemental Movie 2), after ~ 70 min, the cell abruptly migrated off the EG-thiol and continued to spread on the fibronectin region. For the remainder of the experiment, the cell adhered to the fibronectin pattern and did not spread onto the EG-thiol region. The progression of this change in spreading and location was quantified by measuring SPR reflectivity associated with pixels corresponding to areas of EG versus areas of fibronectin as shown in Figure 5B. It is apparent that the cell did not spread appreciably

while associated with EG, and that spreading occurred as contact with EG decreased. These SPR images also provide evidence of close contact between cells and the nonadhesive surface. Although the leftmost cell does not spread appreciably on the EG area, both cells display close interaction of cell processes with the EG substratum.

Lateral ruffling of the cell edge was observed for the vSMC after the cells were fully spread (~ 300 min after cell seeding) (Fig. 6A–C and Supplementary File 3). Time-lapse imaging of a representative cell, 6 h after seeding, shows a lateral ruffle that appears to traverse wave-like along the cell membrane edge (Fig. 6A). These lateral ruffles have an average velocity of 3 – $5 \mu\text{m}/\text{min}$ which is on the same order of magnitude observed for lateral waves in several different cell types and measured by TIRFM (5,32). The same cell continues to exhibit lateral ruffling after 24 h (Fig. 6B) with the measured lateral wave speed being approximately the same as at 6 h. After 24 h in contact with the substratum, the cell-substratum interaction appears to be less spatially homogeneous than it appears immediately after spreading, as observed above (Fig. 3). Figure 6C shows that after 24 h, some cells demonstrate anterograde waves that sporadically appear to be separated from the originating cell-substratum edge. This suggests that cell-substratum contacts can arch over the substratum, where some areas of the cell membrane are in closer contact with the substratum than others, such as appears to occur when cells extend laterally moving lamellipodium. This behavior is consistent with a previously described lamellipodial bending model (33) and suggests the SPRI could be a valuable tool for understanding the details of cell spreading, lamellipodial extension, and cytoskeleton dynamics.

DISCUSSION

SPRI of cells will especially be an useful tool for cell biology research because it requires no fluorescent labels or other exogenous probes to provide highly sensitive contrast between cells and substratum. Because the intensity of the probing light is low, cells can be safely examined for long periods of time. The contrast in an SPR image is due to difference in refractive index, which in biological samples is largely a response to differences in mass of protein and lipid mate-

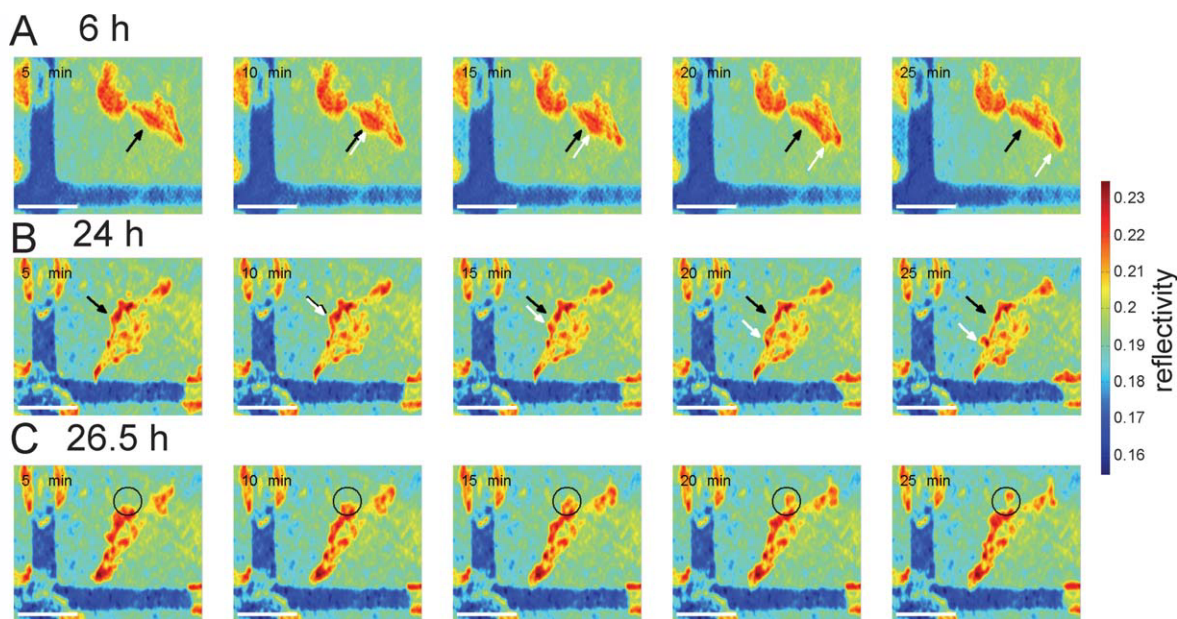


Figure 6. Time dependent measurements of cell ruffling dynamics using SPRI. (A) Time-lapse images of a selected cell every 5 min, 6 h after seeding, shows lateral membrane ruffling (arrow). (B) Time-lapse images of same cell in (A) 24 h after seeding (5-min increments), shows lateral membrane ruffling (arrow) as well as a more heterogeneous cell-substratum contact. (C) Time-lapse series for the same cell in (B) depicting a lateral membrane wave (encircled) that separates from the cell edge, suggesting an arch in the cell-substratum interaction, followed by retraction of the cell edge both inward and upward. The cell-substratum contact is also observed to change during the 2.5 h separating the images collected in (B) and (C). The color bar indicates reflectivity values for the images. Scale bars = 100 μm . [Color figure can be viewed in the online issue, which is available at wileyonlinelibrary.com.]

rial within the penetration depth of the plasmon wave. Because the contrast is approximately proportional to mass, SPRI can be inherently more quantitative than other imaging techniques such as phase or interference contrast. The sensitivity to refractive index differences is on the order of one part in 10^{-6} or better, and so the contrast between background and cell is great; this facilitates the detection of cell edges and processes that may be otherwise difficult to observe with other imaging modalities. Image segmentation of cells is thus enabled, and therefore simple intensity thresholding is an unambiguous method for segmenting cell objects. Because SPRI can also image the underlying extracellular patterned surface, live cell behavior can be monitored as a function of the underlying surface chemistry, and small mass changes in the substratum can be quantified (18).

Rates of cell spreading and lateral ruffling made by SPRI in this study are consistent with those made using techniques such as TIRFM (5,32), but with SPRI, live cells can be examined for longer periods of time, label-free, allowing the progression of cell-surface contacts with time to be continuously measured. In fact, we observe the cell-substratum interactions of the same cell with SPRI over 24 h, a time scale much longer than that typically observed with TIRFM. TIRFM can provide highly sensitive detection, but only of the specifically labeled molecule. In contrast, SPRI, while not as specific or sensitive as TIRFM, allows detection of all proteins and material attached to the surface as well as the cell-substratum contacts. In this study, we also observe changes in the homogeneity of the cellular footprint of vSMC over time. This may be

due to changes in the distance of cellular components from the surface, changes in the intracellular location of proteins, secretion of ECM at the cell-substratum interface, or a combination. Further studies will aim to correlate the SPRI signal with immunochemical identification of cellular components.

CONCLUSION

SPRI has the potential to provide unique insight into cell-substratum interactions that bridge the molecular to macromolecular scale. The technique does not require complicated optical components; it can be performed in conjunction with transmission imaging technique to provide complementary data; it does not require fluorescent labels; and it is applicable for long term live cell studies because of the low levels of visible light required. In contrast, SPRI is based largely on differences in molecular mass of materials within the penetration depth of the plasmon field, which enables quantitation of cell-substratum interactions. Cell spread area is easy to determine because of unambiguous segmentation of cells from background. Changes in the mass of the protein matrix around cells can be determined as we have shown previously (18). The locations, densities, and areas of cell substratum contacts can be easily observed, and the dynamic changes in these features can be followed in individual cells over long periods of time.

LITERATURE CITED

1. Discher DE, Janmey P, Wang YL. Tissue cells feel and respond to the stiffness of their substrate. *Science* 2005;310:1139–1143.
2. Plopper G. The extracellular matrix and cell adhesion. In: Lewin B, Cassimeris L, Lingappa VR, Plopper G, editors. *Cells*. Sudbury: Jones and Bartlett; 2007. pp 645–702.

3. Ruoslahti E, Pierschbacher MD. New perspectives in cell-adhesion—Rgd and integrins. *Science* 1987;238:491–497.
4. Burmeister JS, Olivier LA, Reichert WM, Truskey GA. Application of total internal reflection fluorescence microscopy to study cell adhesion to biomaterials. *Biomaterials* 1998;19:307–325.
5. Dobreiner HG, Dubin-Thaler BJ, Hofman JM, Xenias HS, Sims TN, Giannone G, Dustin ML, Wiggins CH, Sheetz MP. Lateral membrane waves constitute a universal dynamic pattern of motile cells. *Phys Rev Lett* 2006;97:038102(1–4).
6. Verschuere H. Interference reflection microscopy in cell biology—methodology and applications. *J Cell Sci* 1985;75:279–301.
7. Ramsden JJ, Li SY, Heinze E, Prenosil JE. Optical method for measurement of number and shape of attached cells in real time. *Cytometry* 1995;19:97–102.
8. Aref A, Horvath R, McColl J, Ramsden JJ. Optical monitoring of stem cell-substratum interactions. *J Biomed Opt* 2009;14:010501(1–3).
9. Raether H. Surface Plasmons on Smooth and Rough Surfaces and on Gratings. Berlin: Springer-Verlag; 1988. p 136.
10. Altschuh D, Dubs MC, Weiss E, Zederlitz G, Vanregenmortel MHV. Determination of kinetic constants for the interaction between a monoclonal-antibody and peptides using surface-plasmon resonance. *Biochemistry* 1992;31:6298–6304.
11. Peterlinz KA, Georgiadis RM, Herne TM, Tarlov MJ. Observation of hybridization and dehybridization of thiol-tethered DNA using two-color surface plasmon resonance spectroscopy. *J Am Chem Soc* 1997;119:3401–3402.
12. Ziblat R, Lirtsman V, Davidov D, Aroeti B. Infrared surface plasmon resonance: A novel tool for real time sensing of variations in living cells. *Biophys J* 2006;90:2592–2599.
13. Nelson BP, Grimsrud TE, Liles MR, Goodman RM, Corn RM. Surface plasmon resonance imaging measurements of DNA and RNA hybridization adsorption onto DNA microarrays. *Anal Chem* 2001;73:1–7.
14. Borejdo J, Gryczynski Z, Calander N, Muthu P, Gryczynski I. Application of surface plasmon coupled emission to study of muscle. *Biophys J* 2006;91:2626–2635.
15. Gryczynski I, Malicka J, Gryczynski Z, Lakowicz JR. Surface plasmon-coupled emission with gold films. *J Phys Chem B* 2004;108:12568–12574.
16. Abdul Jamil MM, Sefat F, Khaghani SA, Lobo SB, Javid FA, Youseffi M, Britland ST, Liu SG, See CW, Somekh MG, Denyer MCT. Cell imaging with the widefield surface plasmon microscope. In: Osman A, editor. *IFMBE Proceedings*, 4th Kuala Lumpur International Conference on Biomedical Engineering 2008, Volume 21. Kuala Lumpur, Malaysia: Springer Berlin Heidelberg; 2008. pp 528–531.
17. Giebel KF, Bechinger C, Herminghaus S, Riedel M, Leiderer P, Weiland U, Bastmeyer M. Imaging of cell/substrate contacts of living cells with surface plasmon resonance microscopy. *Biophys J* 1999;76:509–516.
18. Peterson AW, Halter M, Tona A, Bhadriraju K, Plant AL. Surface plasmon resonance imaging of cells and surface-associated fibronectin. *BMC Cell Biol* 2009;10:16(1–17).
19. Ulman A. *An Introduction to Ultrathin Organic Films: From Langmuir-Blodgett to Self-Assembly*, Vol. XXIII. Boston: Academic Press; 1991. p 442.
20. Halter M, Tona A, Bhadriraju K, Plant AL, Elliott JT. Automated live cell imaging of green fluorescent protein degradation in individual fibroblasts. *Cytometry A* 2007;71:827–834.
21. Chen CS, Ostuni E, Whitesides GM, Ingber DE. Using self-assembled monolayers to pattern ecm proteins and cells on substrates. In: Streuli C, Grant M, editors. *Extracellular Matrix Protocols, Methods in Molecular Biology*. New Jersey: Humana; 2000. pp 209–219.
22. Peterlinz KA, Georgiadis R. In situ kinetics of self-assembly by surface plasmon resonance spectroscopy. *Langmuir* 1996;12:4731–4740.
23. Kramer M. Evanescent waves in microscopy. *Photonik* 2004;2:42–44.
24. Inoue S, Spring KR. *Video Microscopy: The Fundamentals*. New York: Plenum; 1998. p 741.
25. Brockman JM, Nelson BP, Corn RM. Surface plasmon resonance imaging measurements of ultrathin organic films. *Annu Rev Phys Chem* 2000;51:41–63.
26. Mrksich M. Tailored substrates for studies of attached cell culture. *Cell Mol Life Sci* 1998;54:653–662.
27. Foster B. *Optimizing Light Microscopy for Biological and Clinical Laboratories*. Dubuque: Kendall/Hunt; 1997. p 187.
28. Engvall E, Ruoslahti E. Binding of soluble form of fibroblast surface protein, fibronectin, to collagen. *Int J Cancer* 1977;20:1–5.
29. Hahn LH, Yamada KM. Identification and isolation of a collagen-binding fragment of the adhesive glycoprotein fibronectin. *Proc Natl Acad Sci USA* 1979;76:1160–1163.
30. Singer II, Kazazis DM, Scott S. Scanning electron microscopy of focal contacts on the substratum attachment surface of fibroblasts adherent to fibronectin. *J Cell Sci* 1989;93(Pt 1):147–154.
31. Dimilla PA, Stone JA, Quinn JA, Albelda SM, Lauffenburger DA. Maximal migration of human smooth-muscle cells on fibronectin and type-IV collagen occurs at an intermediate attachment strength. *J Cell Biol* 1993;122:729–737.
32. Machacek M, Danuser G. Morphodynamic profiling of protrusion phenotypes. *Biophys J* 2006;90:1439–1452.
33. Giannone G, Dubin-Thaler BJ, Rossier O, Cai Y, Chaga O, Jiang G, Beaver W, Dobreiner HG, Freund Y, Borisy G, Sheetz MP. Lamellipodial actin mechanically links myosin activity with adhesion-site formation. *Cell* 2007;128:561–75.